

Nonreciprocity Induced Fractional Nonlinear Thouless Pumping

Yanqi Zheng,¹ Kun Pu,¹ Lingqing Ren,¹ Chenxi Bai,¹ and Zhaoxin Liang^{1,*}

¹*Department of Physics, Zhejiang Normal University, Jinhua 321004, China*

Recent interest has surged in eigenvalue's nonlinearity-based topological transport governed by the equation of auxiliary eigenvalues $H\Psi = \omega S(\omega)\Psi$ [T. Isobe *et al.*, *Phys. Rev. Lett.* **132**, 126601 (2024); C. Bai and Z. Liang, **111**, 042201 (2025); *Phys. Rev. A* **112**, 052207 (2025)] rather than the conventional Schrödinger equation $H\Psi = E\Psi$ in conservative settings, yet non-Hermitian generalizations remain uncharted. In this work, we are motivated to investigate the nonlinear Thouless pumping in a non-Hermitian and nonlinear Rice-Mele model. In particular, we uncover how non-Hermiticity parameters can induce fractional topological phases—even in the presence of quantized topological invariants as predicted by conventional linear approaches. Crucially, these fractional phases are naturally explained within the framework of the equation of auxiliary eigenvalues, directly linking nonlinear spectral characteristics to the bulk-boundary correspondence. Our findings reveal novel emergent phenomena arising from the interplay between nonlinearity and non-Hermiticity, providing key insights for the design of topological insulators and the controlled manipulation of quantum edge states in the real world.

I. INTRODUCTION

Thouless pumping [1–3] in linear quantum systems serves as the paradigmatic example of quantized topological transport, where adiabatic cyclic modulation of parameters drives robust charge displacement governed by the TKNN relation [4]. The physical mechanism [5] behind the Thouless pumping demonstrates how topology manifests in periodically driven systems through quantized transport properties, establishing a foundational framework for understanding non-trivial band structures in quantum dynamics. Its experimental realizations encompass ultracold atomic gases [6, 7], photonic systems [8, 9], and spin-based platforms [10], demonstrating exceptional experimental versatility while preserving quantitative agreement with theoretical predictions. Next, nonlinearity, a key ingredient playing out in various distinct disciplines such as physics, biology, chemistry, economics, and social sciences, can induce nonlinear Thouless pumping [11–35]. In more details, nonlinearity induces quantized transport through soliton formation and spontaneous symmetry-breaking bifurcations, contrasting with linear Thouless pumping in electronic systems [1–3] that necessitates complete occupation of an entire linear band. Meanwhile, the quantized nonlinear Thouless pumping [36] can be understood by the Chern number of a Bloch band of the linear Hamiltonian, which constitutes a natural extension of the TKNN relation to nonlinear systems. Additionally, the fractional nonlinear Thouless pumping can occur for a soliton when the linear Hamiltonian is topologically non-trivial [37] or trivial [38], whose transport mechanisms unique to the existence of nonlinearity have gone beyond the framework of TKNN relation.

Recently, the experimental advances across distinct physical platforms—including photonics [39, 40], ultra-

cold atoms [41–43], and acoustic systems [44, 45]—have enabled the controlled realization of non-Hermitian systems, characterized by engineered gain-loss mechanisms or nonreciprocal couplings. These systems exhibit unique topological phenomena absent in Hermitian settings, such as the non-Hermitian skin effect [46–53] and exceptional points [54–68]. Owing to continuous advances in theoretical and experimental techniques [69–99], non-Hermitian topological transport has been widely investigated [100–107]. In these systems, the conventional bulk-boundary correspondence often needs to be extended using concepts like biorthogonal bases or generalized Brillouin zones [47, 108–110] to correctly capture complex spectral features and the localization of skin modes.

While non-Hermiticity can induce linear topological phase transitions, existing research predominantly focuses on stabilizing linear responses. Recent breakthroughs in photonic platforms [111, 112] now enable exploration of non-Hermitian-nonlinear coupling regimes—a critical frontier due to the poorly understood interplay between these two dimensions. This integration introduces profound questions: How do nonlinearity and non-Hermiticity synergistically reshape topological transport mechanisms? Can their interaction engender novel bulk-boundary correspondence paradigms that transcend conventional quantum topology? Resolving these issues holds transformative potential for non-equilibrium quantum simulation, robust photonic devices, and fundamental understanding of open quantum matter.

The second motivation of this work stems from the recent breakthrough in Refs. [113–115], which establishes a direct link between bulk-edge correspondence and eigenvalue nonlinearity in both linear [113] and nonlinear [114, 115] Hamiltonians through an auxiliary eigenvalue equation: $H\Psi = \omega S(\omega)\Psi$. Conceptually going beyond previously conventional approaches [1–3], this formulation reveals how spectral properties of the bulk Hamiltonian H govern nonlinear eigenvalue problems, thereby bridging a unified description of bulk-edge

* Corresponding author: zhxliang@zjnu.edu.cn

physics through the lens of nonlinear eigenvalue problems in Hermitian physical systems. In particular, the auxiliary eigenvalue formulation of $H\Psi = \omega S(\omega)\Psi$ predict observable phenomena [115] inaccessible to conventional linear bulk-edge paradigms [2]. Up to now, the investigations on bulk-edge correspondence based on the framework of nonlinear eigenvalue problems via auxiliary eigenvalues are focused on Hermitian physical systems, however, its counterpart of the non-Hermitian scenario is largely unexplored.

To address the above-mentioned questions, we are motivated to employ a non-Hermitian nonlinear Rice-Mele (RM) model (Fig. 1(a)) characterized by nonlinearity of g and non-Hermiticity of γ , to systematically investigate topological transport in a non-Hermitian nonlinear environment. We first separately calculate the relationship between the system's Chern number \mathcal{C} and the non-Hermitian parameter γ under linear ($H\Psi = E\Psi$) and nonlinear eigenvalue ($H\Psi = \omega S(\omega)\Psi$) conditions (Fig. 1(b)). Surprisingly, we identify parameter regimes where the non-Hermiticity parameter γ induces fractional topological phases, as explained within the auxiliary eigenvalue framework. This occurs even in the presence of quantized topological invariants—predicted by conventional linear approaches—highlighting a counterintuitive deviation from traditional topological paradigms. Subsequently, numerical simulations tracking soliton center-of-mass trajectories under adiabatic conditions reveal pumping dynamics where combined non-Hermitian and nonlinear parameters induce transitions from integer to fractional Chern phases (Fig. 5(a)). The latter phenomenon demonstrates how eigenvalue nonlinearities generate observable bulk-boundary correspondences absent in conventional linear frameworks, establishing a novel paradigm for topological transport in the non-Hermitian and nonlinear systems. Our results predict that fractional non-Hermitian nonlinear Thouless pumping can be realized in photonic waveguides and cold-atom systems, opening new avenues for investigating topological states in non-equilibrium open systems.

This paper is structured as follows: In Sec. II A, we introduce the non-Hermitian nonlinear RM model. Sec. II B presents the calculation and analysis of the Chern number under both linear and nonlinear eigenvalue conditions. The derivation of the underlying nonlinear Schrödinger equation is detailed in Sec. III A, while Sec. III B employs the instantaneous soliton method to analyze the associated energy spectrum and phase diagram. Building upon this theoretical framework, Sec. IV provides detailed numerical results of the soliton displacements and energy spectra, elucidating the distinct impacts of non-Hermiticity and nonlinearity. The bulk-boundary correspondence of the model and the regulatory roles of both non-Hermitian and nonlinear effects on topological edge states are elaborated in Sec. V. Finally, Sec. VI summarizes the main findings and discusses their implications for future studies.

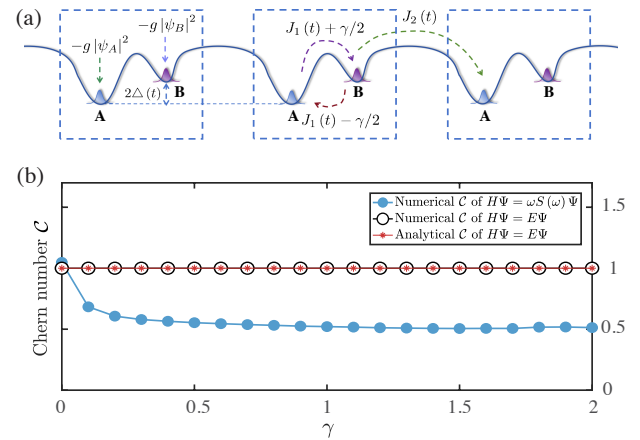


Figure 1. (a) Schematic of the nonlinear non-Hermitian RM model. The dashed box indicates a unit cell consisting of sublattice A and B. (b) Chern number \mathcal{C} as a function of γ for $g = 0$. The Chern numbers for the linear eigenvalue problem $H\Psi = E\Psi$, computed analytically and numerically, are shown by the red star and black hollow circle, respectively. The blue solid circle represents the Chern number for the nonlinear problem $H\Psi = \omega S(\omega)\Psi$, obtained numerically. The relevant parameters are given as: $J = 1$, $\delta = 0.5$, $\Delta = 1$, $T = 2000\pi$, $\omega = \omega_d = 10^{-3}$.

II. NONLINEAR NON-HERMITIAN RICE-MELE MODEL

A. Model system

In this work, we are interested in a one-dimensional interacting bosonic chain containing N dimerized units (see Fig. 1(a)), where each unit consists of two distinct lattice sites labeled A and B. Within mean-field approximation, the system's static and dynamic properties are governed by a non-Hermitian generalization of the nonlinear RM Hamiltonian H_{RM} [16, 114, 115], augmented with additional non-Hermitian terms H_{NH} proposed in Ref. [107]. The total Hamiltonian of our model system then reads

$$H_{\text{RM}} = \sum_{n=1}^{N-1} (J_1 \Psi_{n,A}^* \Psi_{n,B} + J_2 \Psi_{n,B}^* \Psi_{n+1,A} + \text{H.c.}) - \Delta \cos(\omega_d t) \sum_{n=1}^N (|\Psi_{n,A}|^2 - |\Psi_{n,B}|^2) - \frac{g}{2} \sum_{n=1}^N (|\Psi_{n,A}|^4 + |\Psi_{n,B}|^4), \quad (1)$$

$$H_{\text{NH}} = \sum_{n=1}^N \frac{\gamma}{2} (\Psi_{n,A}^* \Psi_{n,B} - \Psi_{n,B}^* \Psi_{n,A}). \quad (2)$$

In Eqs. (1) and (2), for each unit cell consisting of two sublattices denoted as A and B, where $\Psi_{n,A}$ and $\Psi_{n,B}$ correspond to the wavefunction on the A and B sublattices within the n -th unit cell, respectively. The time-dependent intra-cell and inter-cell hopping strengths are

given by $J_1 = -J - \delta \sin(\omega_d t)$ and $J_2 = -J + \delta \sin(\omega_d t)$. The parameter J sets the uniform hopping amplitude, δ controls the modulation amplitude, and ω_d is the modulation frequency. To ensure adiabatic evolution, we require $\omega_d \ll J, \delta$. The term $\Delta \cos(\omega_d t)$ represents a time-varying step-like on-site potential with magnitude Δ . Nonlinear interactions are incorporated via a Kerr-type term of strength g [16, 114, 115]. The coefficient γ in Eq. (2) quantifies the non-reciprocal character of the hopping process. The emphasis and value of this work is to investigate how the non-Hermitian nature captured by Hamiltonian (2) can affect the topological properties of nonlinear RM model of Hamiltonian (1).

Before exploring non-Hermitian effects labelled by γ in Eq. (2) on the nonlinear RM model, we would like to establish the basic properties [16, 114, 115] of nonlinear RM model by setting $\gamma = 0$. Compared with linear RM model [116], the introduction of nonlinearity of g in Eq. (1) has brought rich dynamics into topological phases, typical of nonlinear integer [11–33] or fractional Thouless pumping [37, 38]. In more details, nonlinearity acts to quantize transport via soliton formation and spontaneous symmetry-breaking bifurcations. In exploring physics arising from the interplay of nonlinearity and topology, the Thouless pumping of such solitons has been experimentally observed [11, 34, 35], and theoretically studied in both the weak nonlinear regime and the strong nonlinear regime [13–16, 114, 115].

Furthermore, incorporating additional non-Hermitian terms described by Hamiltonian (2) into the nonlinear RM model of Hamiltonian (1) induces non-equilibrium dynamics, manifesting two key features: (1) Topological invariants require biorthogonal-basis calculations, potentially altering system topology; (2) Non-Hermitian skin effects localize eigenstates at boundaries. These points immediately suggest two novel implications of nonlinear Thouless pumping: (i) Emergent bulk-boundary correspondences in non-Hermitian nonlinear regimes; (ii) Skin-characterized solitons under specific parameter conditions. These predictions align with recent experiments realizing nonlinear skin solitons [117] and Hopf bifurcation-induced criticality in non-Hermitian skin effects [118].

B. Non-Hermitian Chern number

The topological properties of the nonlinear non-Hermitian RM model described by Eqs. (1) and (2) are governed by four key parameters: nearest-neighbor coupling strengths J_1 and J_2 , nonreciprocal parameter γ , and nonlinear interaction strength g . This work reveals that the synergistic interplay between non-Hermitian skin effects and nonlinear band engineering unveils novel bulk-edge correspondences, enabling exploration of exotic phenomena beyond conventional linear Hermitian frameworks. Specifically, we demonstrate that γ -induced directional amplification and g -mediated

interaction-induced gap openings govern phase transitions through a competitive mechanism, while establishing topological-protected channels for solitonic excitations. These results establish a paradigm for engineering non-Hermitian topological phases via coupled nonlinear-dispersion mechanisms, holding promise for photonic and quantum simulator platforms with reconfigurable boundary states.

As the first step, we derive the topological invariants for the linearized non-Hermitian RM model with $g = 0$ in Eq. (1). For periodic boundary conditions, the momentum-space wavefunctions for each sublattice follow from discrete Fourier transformation as $|\Psi_{A(B)}(k, t)\rangle = 1/\sqrt{N} \sum_{j=1}^N e^{ikj} |\Psi_{j,A(B)}(t)\rangle$ with $k = 2\pi m/N$ and $m = 0, 1, \dots, N - 1$. The total wavefunction is expressed as a two-component spinor $|\Psi(k, t)\rangle = (|\Psi_A(k, t)\rangle, |\Psi_B(k, t)\rangle)^T$, and then the momentum-space form of Hamiltonian (1) and (2) can be written in the form of $H = \sum_k \langle \Psi(k, t) | H(k, t) | \Psi(k, t) \rangle$. Here, the single-particle Hamiltonian $H(k, t)$ can be written as

$$H(k, t) = d_x \sigma_x + (d_y + i \frac{\gamma}{2}) \sigma_y + d_z \sigma_z, \quad (3)$$

with $d_x = J_1 + J_2 \cos k$, $d_y = J_2 \sin k$, $d_z = -\Delta \cos \omega t$ and $\sigma_{x,y,z}$ representing the Pauli matrices. The topological properties of our model system can be characterized by the Chern number

$$\mathcal{C} = \frac{1}{2\pi} \int_0^{2\pi/\omega_d} dt \int_{-\pi}^{\pi} dk \Omega(k, t), \quad (4)$$

where $\Omega(k, t)$ is the Berry curvature. In non-Hermitian systems, we adopt the definition of $\Omega(k, t)$ [46–53] in the biorthogonal basis as detailed in Appendix A

$$\Omega = i \langle \partial_t u_L | \partial_k u_R \rangle - i \langle \partial_k u_L | \partial_t u_R \rangle. \quad (5)$$

Here, $|u_R(k, t)\rangle$ and $|u_L(k, t)\rangle$ are the eigenstates of $H(k, t)$ and $H^\dagger(k, t)$ in Eq. (3), respectively. In general, as long as the energy gap of Hamiltonian (3) remains open during the adiabatic evolution, the Chern number \mathcal{C} defined in Eq. (4) can ensure the quantization of the charge transfer in each pumping cycle.

Next, we need to obtain the biorthogonal eigenstates of $|u_{L(R)}\rangle$ in Eq. (5) in order to calculate the Chern number in Eq. (4). As pointed out in Refs. [113–115, 119], two kinds of scenarios of calculating $|u_{L(R)}\rangle$ can be adopted

(i) In the first scenario, one can obtain the biorthogonal eigenstates of $|u_{L(R)}\rangle$ based on the linear Hamiltonian $H\Psi = E\Psi$ in the traditional quantum mechanics. Based on the definitions of Chern number \mathcal{C} in Eq. (4), we proceed to analytically calculate the Chern numbers for different values of γ , as shown by the red stars in Fig. 1(b). It can be seen from the figure that the system always remains in a topologically nontrivial state with $\mathcal{C} = 1$. To verify the analytical results, we also employ a numerical method based on the Wilson loop to calculate the Chern number [114, 115], the results of which are represented by

the black hollow circles in Fig. 1(b). The consistency between the Chern numbers obtained by the two methods indicates that the Wilson loop method [120] is not only reliable but also more convenient in practical calculations and can accurately reflect the topological properties of the system.

(ii) The second scenario is referred to as the nonlinear eigenvalue equation defined as follows [113–115]:

$$H(k, t)\Psi = \omega S(\omega)\Psi. \quad (6)$$

Then we define the auxiliary matrix $P(\omega, k) = H(k, t) - \omega S(\omega)$. At this point, the nonlinear equation is transformed into the auxiliary equation $P(\omega, k)\Psi = \lambda\Psi$. Here, $S(\omega) = I - M_S\sigma_z$, and $M_S(\omega) = M_1 \tanh(\omega t)$, where $M_S(\omega)$ reflects the dependence on nonlinearity. At this stage, the frequency ω becomes a parameter, while the eigenvalues λ of the auxiliary equation form the energy bands. Only when $\lambda = 0$ do the solutions of the auxiliary equation coincide with those of Eq. (6), and the corresponding ω represents the physical eigenfrequency of the system. From a physical standpoint, therefore, we only need to focus on the case $\lambda = 0$. By constructing an auxiliary linear eigenvalue problem, we can analyze and predict the topological edge states of the physical nonlinear eigenvalue problem, thereby establishing a bulk-edge correspondence tailored to nonlinear systems. The Chern numbers calculated via this second method for different γ values are shown as blue circles in Fig. 1(b).

Finally, the results of Chern number in Eq. (4) calculated above two scenarios are all displayed in Fig. 1(b). In more details, the red stars represent the analytical Chern numbers based on linear eigenvalues, while the black hollow circles and blue solid circles represent the numerical Chern numbers corresponding to linear eigenvalues and nonlinear eigenvalues, respectively. It is worth noting that the calculations of both linear and nonlinear eigenvalues are performed under the condition of $g = 0$. As can be seen from Fig. 1(b), the Chern number remains at

$\mathcal{C} = 1$ in the linear case, while under the nonlinear eigenvalue problem, the Chern number exhibits fractional behavior and gradually stabilizes at $\mathcal{C} = \frac{1}{2}$. This behavior can be understood as the geometric phase of the effective Bloch bands being reconstructed under the combined action of strong nonlinearity and non-Hermitian coupling, leading to the coupling and excitation of multiple topological bands and resulting in fractional Chern numbers. Based on the above results, when non-Hermitian nonlinearity is introduced (blue circles in Fig. 1(b)), solitons [115] are expected to exhibit fractional pumping phenomena. In contrast, such fractional pumping behavior is completely absent in the linear case (red stars and black circles in Fig. 1(b)).

III. TOPOLOGICAL PHASE DIAGRAM OF NON-HERMITIAN AND NONLINEAR RM MODEL

A. Nonlinear Schrödinger equation

In Sec. II, we have mentioned that for the non-Hermitian nonlinear Hamiltonian with $g \neq 0$, the nonlinear term can form solitons within the lattice. Therefore, in the scenario described by Fig. 1(a) (blue circles), we predict that solitons will exhibit fractional pumping behavior. Our strategy for demonstrating the physical manifestations of the fractional Chern number within the nonlinear framework (Fig. 1(b)) is inspired by the concept of nonlinear Thouless pumping [3, 11–22]. Specifically, we expect that the soliton supported by Hamiltonian (1) and (2) will undergo fractional pumping in the scenario depicted in Fig. 1(b).

To investigate the dynamical behavior of solitons governed by the Hamiltonians (1) and (2), we derive the corresponding equations of motion through $i\partial\Psi_j/\partial t = \delta H/\delta\Psi_j^*$ [114, 115]. Specifically, the system evolution of Ψ_j is governed by the discrete nonlinear non-Hermitian Schrödinger equations as follows,

$$i\frac{\partial\Psi_{j,A}}{\partial t} = -\left(J + \delta \sin \omega_d t - \frac{\gamma}{2}\right)\Psi_{j,B} - \left(J - \delta \sin \omega_d t + \frac{\gamma}{2}\right)\Psi_{j-1,B} - \left(\Delta \cos \omega_d t + g|\Psi_{j,A}|^2\right)\Psi_{j,A}, \quad (7)$$

$$i\frac{\partial\Psi_{j,B}}{\partial t} = -\left(J + \delta \sin \omega_d t - \frac{\gamma}{2}\right)\Psi_{j,A} - \left(J - \delta \sin \omega_d t + \frac{\gamma}{2}\right)\Psi_{j-1,A} + \left(\Delta \cos \omega_d t - g|\Psi_{j,B}|^2\right)\Psi_{j,B}, \quad (8)$$

where $j = 1, 2, \dots, N-1, N$ labels the lattice sites. Eqs. (7) and (8) define a discrete nonlinear non-Hermitian Schrödinger system, which is fundamentally equivalent to the lattice Gross-Pitaevskii equation describing Bose systems with nonlinear interactions and non-Hermitian characteristics. This framework effectively models nonequilibrium dynamics of ultracold atomic gases in optical lattices and optical pulse propagation in photonic crystals with engineered gain/loss profiles [34, 35].

B. Soliton displacement phase diagram

In this subsection III B, we plan to focus on the two phenomena predicted by the Chern number in Fig. 1(b), i.e. the quantized and fractional nonlinear Thouless pumping by numerically solving Eqs. (7) and (8) with the fixed parameters are $J = 1$, $\delta = 0.5$, and $\Delta = 1$ within the parameter regimes of $1 \leq g \leq 10$ and $-2 \leq \gamma \leq 2$. The system employs open boundary conditions ($\Psi_1 = \Psi_{2N} = 0$), and the lattice size

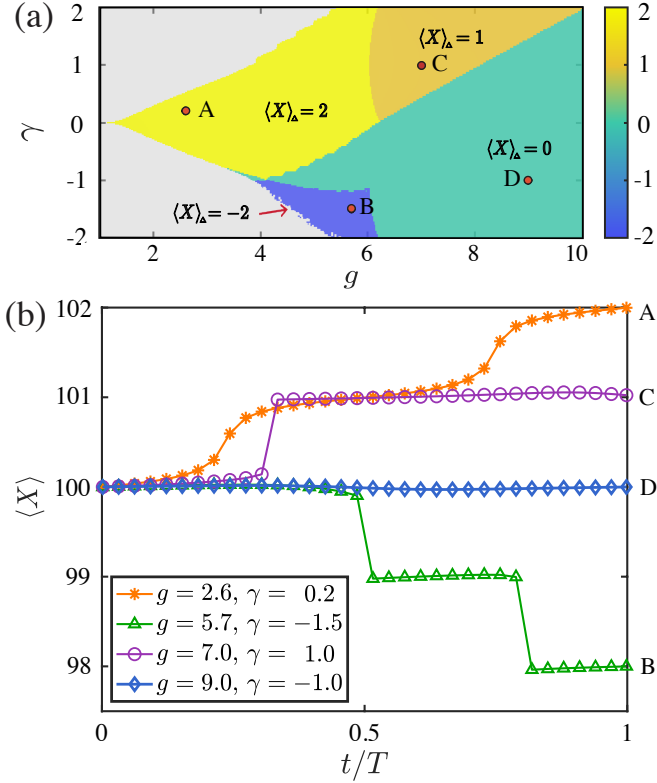


Figure 2. (a) The phase diagram of the soliton centroid transport variation calculated under the scanned parameters (g, γ) . (b) The centroid transport conditions corresponding to the four points marked in Fig. 2(a). The relevant parameters are given as: A $(2.6, 0.2)$, B $(5.7, -1.5)$, C $(7.0, 1.0)$, D $(9.0, -1.0)$. Fixed parameters: $J = 1$, $\delta = 0.5$, $\Delta = 1$, $T = 2000\pi$, $\omega = 10^{-3}$.

is $N = 100$ cells (a total of 200 lattice sites). To verify the reliability of the numerical results, we have ensured that all simulation results are independent of system size through finite-size analysis. All physical quantities in the text have been nondimensionalized. At the initial moment, a soliton state is placed at lattice site $n = 100$. The construction of this soliton state employs the iterative self-consistent algorithm proposed in the ref-

erence literature, with the trial wave function taken as $\Psi_0 = \text{sech} [|x - 100|/5]$. The soliton wave function at each moment is then calculated using the equations. For specific implementation details, see Appendix B. Based on the numerical methods [114, 115], we can study the pumping dynamics of the soliton by monitoring the evolution of its centroid position over time, where the centroid position is defined as $\langle X \rangle = \sum_j j |\Psi_j|^2$.

In Fig. 2, we present the topological phase diagrams by calculating the soliton's displacement of $\langle X \rangle_\Delta$ through numerically solving Eqs. (7) and (8) with different values of the nonlinearity of g and the non-Hermitian parameter of γ . As demonstrated in Fig. 2(a), nonlinear Thouless pumping exhibits four distinct transport regimes, color-coded according to $\langle X \rangle_\Delta = \pm 2, 1$ and 0 respectively. These regimes correspond to three kinds of fundamentally different dynamical responses under periodic parameter modulation. The case of quantized nonlinear Thouless pumping characterized $\langle X \rangle_\Delta = \pm 2$ in Fig. 2(a) means that the soliton is transported by 2 sites per cycle and corresponds to Chern number $\mathcal{C} = \pm 1$ (see black-circle curve in Fig. 1(b)), satisfying with the TKNN relation. In contrast, the case of fractional nonlinear Thouless pumping characterized $\langle X \rangle_\Delta = 1$ in Fig. 2(a) means that the soliton is transported by 1 sites per cycle and corresponds to Chern number $\mathcal{C} = \pm \frac{1}{2}$ (see blue curve in Fig. 1(b)), breaking the TKNN relation by the interplay between g and γ . Note that the gray area corresponds to the non-Hermitian skin effect of soliton's transport. In more details, we select four points in above four distinct regions, labeled as A, B, C, and D, and monitor how soliton's displacements change over time within one pumping cycle in Fig. 2(b). It's evident that soliton's displacements of $\langle X \rangle_\Delta$ indeed are transported to $\langle X \rangle_\Delta = \pm 2, 1$ and 0 as they are expected.

IV. NON-HERMITIAN-INDUCED FRACTIONAL THOULESS PUMPING IN NON-HERMITIAN AND NONLINEAR RM MODEL

In Sec. III, we introduced the discrete non-Hermitian nonlinear Schrödinger equations (7) and (8), and drew the phase diagram of soliton displacement varying with parameters based on these two equations. In Sec. IV, we will more carefully analyze the effects of non-Hermiticity on the energy spectrum and soliton transport behavior of the nonlinear RM model, and explore the role that non-Hermiticity plays on.

First, we analyze the real and complex energy spectra alongside soliton centroid trajectories for parameters at points A-D in Fig. 2(a), demonstrating four distinct dy-

namical regimes. In the weakly nonlinear regime (small g , Figs. 3(a1)-(a3)), the energy spectrum remains entirely real. Remarkably, introducing a finite non-Hermitian parameter γ preserves the soliton displacement of 2 over one pumping cycle, identical to the Hermitian case. This invariance indicates that topological transport properties remain robust against weak non-Hermiticity in this nonlinear regime.

The quantized transport of solitons observed in Fig. 3(a3) directly arises from the Chern number of the non-interacting band structure ($g = 0$). In the weakly

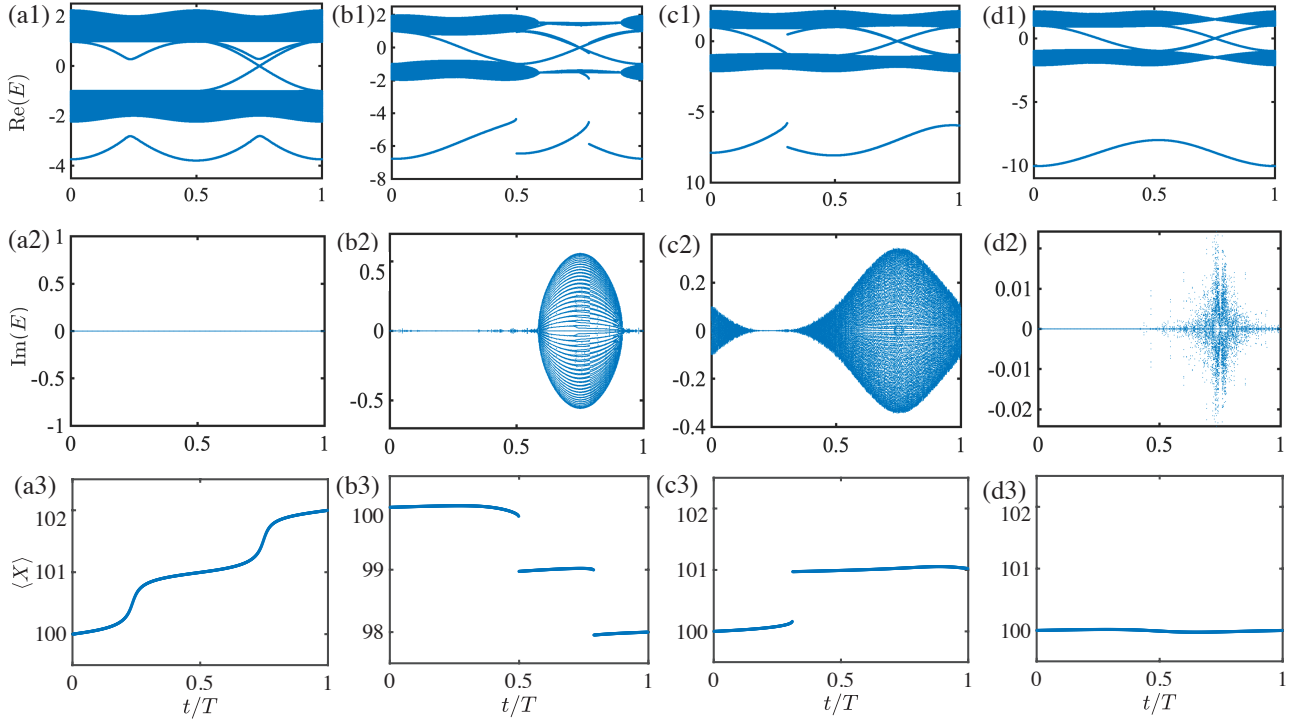


Figure 3. (a1)-(d1): The real energy spectrum structure corresponding to the nonlinear non-Hermitian RM Hamiltonian; (a2)-(d2): The complex energy spectrum structure corresponding to the nonlinear non-Hermitian RM Hamiltonian; (a3)-(d3) The variation of the soliton centroid position expectation value $\langle X \rangle$ with time over a period. The relevant parameter values are: $J = 1$, $\delta = 0.5$, $\Delta = 1$, $T = 2000\pi$, $\omega = 10^{-3}$. In (a1)-(d1)[(a2)-(d2),(a3)-(d3)], the interaction strength and the non-Hermitian strength are taken as $g = 2.6$, $\gamma = 0.2$; $g = 5.7$, $\gamma = -1.5$; $g = 7.0$, $\gamma = 1.0$; and $g = 9.0$, $\gamma = -1.0$, respectively.

nonlinear regime, solitons localize in the lowest energy band ($\mathcal{C} = 1$, see Fig. 1(b)), maintaining quantized displacement through bulk-boundary correspondence. This manifests as a quantized displacement of two lattice sites per pumping cycle, demonstrating the robustness of topological transport against non-Hermitian perturbations. At strong nonlinearities (Fig. 3(d3)), band splitting induces Rabi oscillations between split bands, revealing the breakdown of topological protection. Since the total Chern number of the two bands sums to 0, the net displacement of the soliton vanishes, and the transport process is completely suppressed. In the moderate nonlinearity regime, however, the position jumps observed in the soliton trajectory (see Fig. 3(d3)) arise from the ring structure of the bands, which disrupts the adiabatic evolution path. Introducing non-Hermiticity at this point induces significant non-Hermitian effects: under the parameters of Fig. 3(d), while the absolute value of the soliton transport distance remains unchanged, its direction is reversed, and the energy spectrum acquires an imaginary component. This phenomenon underscores the critical role of non-Hermiticity in shaping the system's dynamical behavior—specifically, the complexification of the energy spectrum and the reversal of the pumping direction are directly tied to the modulation of the Bloch band's geometric phase by the non-Hermitian parameter.

Fig. 3(c3) demonstrates non-Hermiticity-induced fractional soliton pumping, where the soliton exhibits half-integer displacement per pumping cycle under the parameters shown. This behavior emerges from altered bulk-boundary correspondence that develops when non-Hermiticity modifies the system's topology, creating a distinct transport regime absent in the linear regime. The fractional pumping arises from the interplay between non-Hermitian skin effects and modified band structures, as predicted by the non-Bloch Chern number calculations in Fig. 1(b).

Next, following the observation of the predicted fractional transport phenomenon in Fig. 1(b) and Fig. 2(a), we investigate the effect of the non-Hermitian parameter γ in Eq. (2) on the quantized transport of solitons, while keeping the moderate nonlinearity fixed at $g = 5$. Our systematic analysis through Fig. 4 reveals three key regimes: (i) In the Hermitian limit of $\gamma = 0$, the system exhibits the typical nonlinear RM model behavior as shown by the black solid curve in Fig. 4(e), with position jumps during soliton pumping arising from band self-intersections induced by nonlinearity. (ii) In the moderate regime of $\gamma = 0$, as the value of γ increases (see the circle and triangle curve in Fig. 4(e)), the pumping behavior remains stable, with integer-quantized displacement of 2 lattice sites per cycle. This indicates that mod-

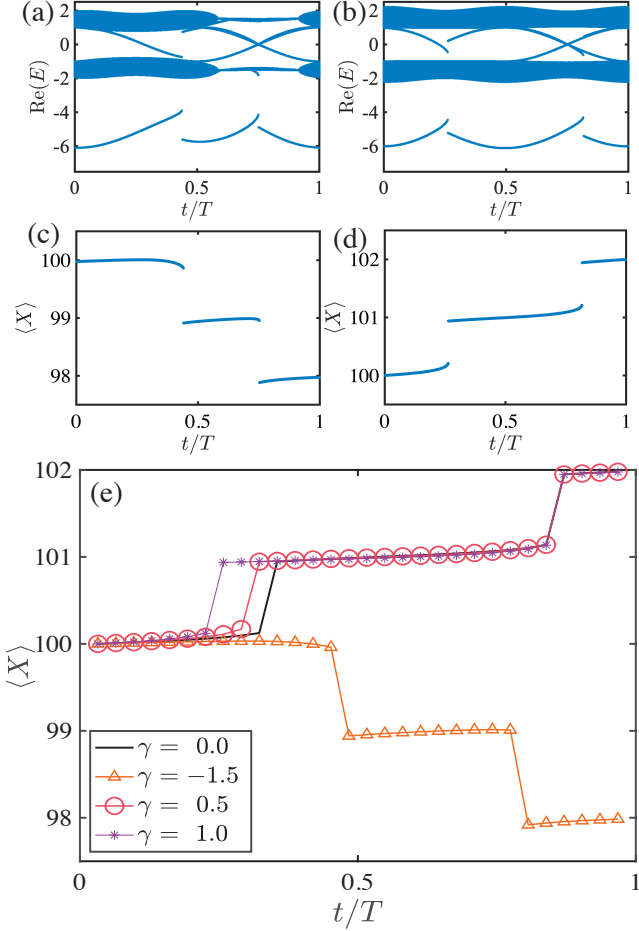


Figure 4. Non-Hermitian control of topological transport: (a,b) Real Part of the Non-Hermitian Nonlinear Eigenvalue Spectrum; (c,d,e) Quantized Soliton Dynamics. Fixed parameters: $g = 5$, $J = 1$, $\delta = 0.5$, $\Delta = 1$, $T = 2000\pi$, $\omega = 10^{-3}$.

erate non-Hermiticity does not alter the system's underlying topological properties, consistent with the robustness of bulk-boundary correspondence in non-Hermitian topological systems. (iii) In the regime of $\gamma < 0$, when γ decreases below a critical threshold, the pumping direction reverses while the absolute value of the displacement remains 2, indicating that non-Hermiticity mainly affects the transport direction without changing its quantized characteristics.

Finally, we present results for the regime where bulk-boundary correspondence undergoes qualitative changes, studied at strong nonlinearity ($g = 8$). At $\gamma = 0$ in the Hermitian limit, the system exhibits significant soliton localization, and topological pumping is completely suppressed. Introducing a finite non-Hermiticity ($\gamma \neq 0$) reactivates topological transport, even in this strongly nonlinear regime. For subthreshold values of γ (below a critical threshold), the system retains behavior analogous to the Hermitian case, with negligible changes in soliton dynamics. However, when γ exceeds this thresh-

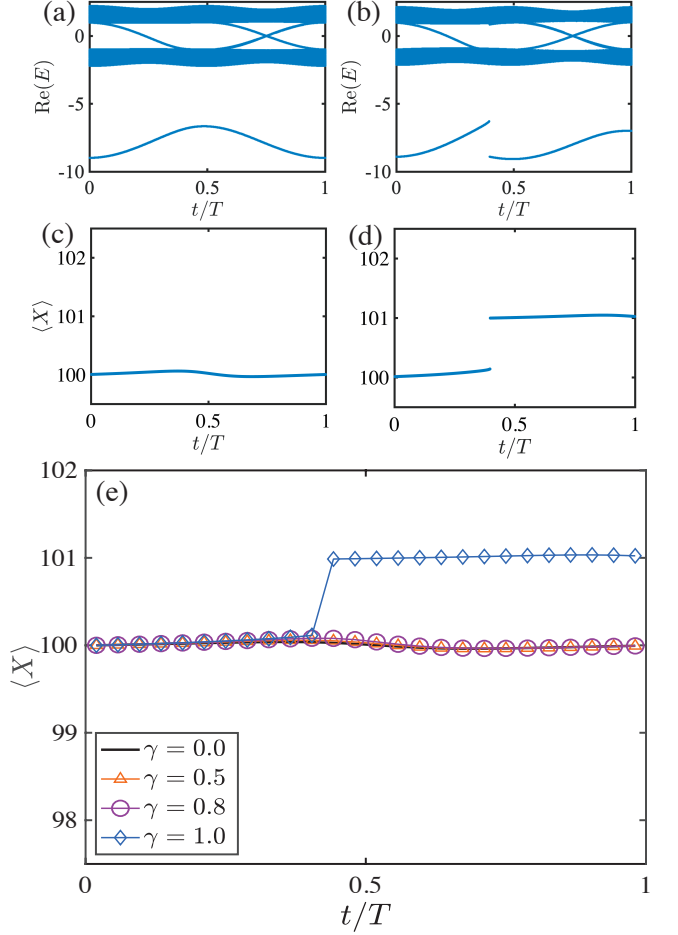


Figure 5. Non-Hermitian modulation of topological transport: (a,b) Real Part of the Non-Hermitian Nonlinear Eigenvalue Spectrum; (c,d,e) Quantized Soliton Dynamics. Fixed parameters: $g = 8$, $J = 1$, $\delta = 0.5$, $\Delta = 1$, $T = 2000\pi$, $\omega = 10^{-3}$.

old, the system enters a fractional quantum pumping regime, characterized by half-integer displacement of solitons per pumping cycle. The transport trajectories obtained via the instantaneous soliton method (Fig. 5(d)) clearly visualize this fractional pumping process, providing direct evidence that non-Hermitian terms can reconstruct the system's effective topological structure in the presence of strong nonlinearity. This reconstruction enables the emergence of fractional transport phenomena, which are absent in the Hermitian limit and highlight the profound impact of non-Hermiticity on topological pumping in nonlinear systems.

V. NON-HERMITIAN NONLINEAR BULK-BOUNDARY CORRESPONDENCE

In Sec. V, we systematically investigate the energy spectrum structure and soliton pumping images of the system under different parameters in the non-Hermitian nonlinear RM model. This section will further elaborate

on the corresponding physical mechanism behind it—the bulk-edge correspondence.

Based on Eqs. (7) and (8), we have drawn the phase diagram shown in Fig. 2 by plotting the soliton displacement results obtained by scanning the parameters (g, γ) . In the weakly and moderately nonlinear regions, changing the non-Hermitian parameter γ does not affect the quantized value of the pumping. The integer quantization behavior can be predicted by the Chern number in the linear limit (corresponding to the $\mathcal{C} = 1$ indicated by the black circles in Fig 1(b)). In the strongly nonlinear region, however, adjusting γ can induce fractional quantum transport of the soliton. In this case, the pumping quantity is no longer an integer and is predicted by the Chern number calculated from the nonlinear eigenvalues (corresponding to the $\mathcal{C} = \frac{1}{2}$ indicated by the blue circles in Fig. 1(b)).

It is particularly noteworthy that the emergence of fractional transport strongly depends on the combined effect of nonlinearity and non-Hermiticity. As shown in Figs. 4 (e) and 5 (e), in the Hermitian case ($\gamma = 0$), adjusting the nonlinearity strength g alone does not induce fractional pumping. Correspondingly, under weakly nonlinear conditions, even in the presence of non-Hermiticity, the system still exhibits integer quantum transport as shown in Fig. 4 (e). This indicates that only when strong nonlinearity and non-Hermiticity coexist can the band structure and geometric properties of the wave functions of the system be changed sufficiently significantly to support topologically nontrivial fractional pumping behavior as displayed by the square curve in Fig. 5 (e).

VI. CONCLUSION AND OUTLOOK

In summary, we investigate the energy spectrum characteristics and soliton dynamics of the nonlinear non-Hermitian RM model, highlighting non-Hermitian effects. By analyzing soliton dynamics via time-dependent evolution equations under combined nonlinear and non-Hermitian conditions, we observe fractionalized topological transport emerging when strong nonlinearity coexists with finite non-Hermitian strength. This phenomenon defies conventional linear/Hermitian frameworks but can be quantitatively predicted by non-Hermitian Chern numbers derived from auxiliary eigenvalues. Our results establish a generalized bulk-edge correspondence for nonlinear non-Hermitian systems, revealing how nonlinear interactions synergize with non-Hermitian effects to induce exotic topological transport. These findings advance the understanding of non-equilibrium topological phases and provide a theoretical foundation for controlling topological transport in photonic waveguides and ultracold atomic systems through combined nonlinearity and non-Hermiticity.

We remark that this work together with the previous Refs. [113–115] establishes a comprehensive description of nonlinear eigenvalue-driven topological transport

through the auxiliary eigenvalue equation $H\Psi = \omega S(\omega)\Psi$ in both conservative and nonconservative settings. This approach elucidates the synergistic mechanisms through which interactions, topology, and dissipation collectively enable novel non-equilibrium paradigms for topological phenomena. The derived bulk-edge correspondence demonstrates how nonlinear spectral characteristics govern boundary state emergence, providing a predictive framework absent in conventional linear theories. These findings advance the understanding of nonequilibrium quantum matter and offer a systematic methodology for engineering topological transport in photonic and atomic systems through combined nonlinearity and non-Hermiticity.

ACKNOWLEDGEMENTS

We thank Ying Hu, Yapeng Zhang, Xuzhen Cao, Shujie Cheng, and Biao Wu for stimulating discussions and useful help. We sincerely acknowledge Yucan Yan for his dedicated efforts during the critical inception phase of this project. This work was supported by the Zhejiang Provincial Natural Science Foundation of China under Grant No. LZ25A040004 and the National Natural Science Foundation of China under Grant No. 12574301.

Appendix A: Chern number

In the Appendix A, we provided the definitions of the Berry curvature in Eq. (5) of the main text according to the biorthogonal basis of $|u(k)\rangle_R$ and $|u(k)\rangle_L$, reading

$$\begin{aligned} \Omega_{kt}^{\alpha\beta} = & i \langle \partial_t u^\alpha(k, t) | \partial_k u^\beta(k, t) \rangle \\ & - i \langle \partial_k u^\alpha(k, t) | \partial_t u^\beta(k, t) \rangle, \end{aligned} \quad (A1)$$

with the normalization condition $\langle u_k^\alpha | u_k^\beta \rangle = 1$ and $\alpha, \beta \in \{L, R\}$. When numerically calculating the Chern number, we employed an equivalent variant of Eq. (4) of the main text. Previous studies have demonstrated that [55, 101], despite having different definition in these Berry curvatures of $\Omega_{kt}^{\alpha\beta}$, they yield the same Chern number when integrated over the momentum-time manifold. For example, we have

$$\mathcal{C} = \int_0^{\frac{2\pi}{\omega_d}} dt \int_{-\pi}^{\pi} dk \Omega_{kt}^{RR} = \int_0^{\frac{2\pi}{\omega_d}} dt \int_{-\pi}^{\pi} dk \Omega_{kt}^{LR}. \quad (A2)$$

Using Ω_{kt}^{RR} for the calculation will bring many conveniences.

Appendix B: Numerical method

To find the steady-state solutions of Eqs. (7) and (8) at any given time, we employ a self-consistent iterative

method. For a given non-Hermitian nonlinear Hamiltonian H , the iterative steps from state $|\Psi_n(t)\rangle$ to state $|\Psi_{n+1}(t)\rangle$ at a specific time t are as follows:

First, based on $|\Psi_n(t)\rangle$, one can obtain the corresponding instantaneous Hamiltonian of $H_n = H(|\Psi_n\rangle, t)$ at the given time of t .

Next, one can solve for the eigenstates $|\psi_i\rangle$ of H_n with $i = q, \dots, 2N$.

Finally, one can select the eigenstate $|\psi_i\rangle$ with the largest overlap with the previous eigenstate $|\Psi_n\rangle$ as the new state, i. e. for all i , $\langle \Psi_n(t) | \psi_{i0} \rangle \geq \langle \Psi_n(t) | \psi_i \rangle$. Repeat the iterative process until the overlap between the new state and the previous state reaches $1 - \langle \Psi_{n+1}(t) | \Psi_n(t) \rangle < 10^{-10}$. The method is highly sen-

sitive to the choice of the initial state, so the selection of the initial state must be done with caution.

We remark that when the non-Hermitian strength exceeds a critical threshold, the non-Hermitian skin effect dominates, resulting in only the boundary-localized state with the largest overlap persisting. This phenomenon explains the emergence of skin solitons at the boundary and the origin of the gray region in Fig. 2. The non-Hermitian and nonlinear effects exhibit competitive interplay: under skin-soliton-producing conditions, increasing the nonlinearity strength suppresses boundary localization, enabling the observation of solitons at the system center.

[1] D. J. Thouless, Quantization of particle transport, *Phys. Rev. B* **27**, 6083 (1983).

[2] Q. Niu and D. J. Thouless, Quantised adiabatic charge transport in the presence of substrate disorder and many-body interaction, *J. Phys. A: Math. Gen.* **17**, 2453 (1984).

[3] R. Citro and M. Aidelsburger, Thouless pumping and topology, *Nat. Rev. Phys.* **5**, 87 (2023).

[4] D. J. Thouless, M. Kohmoto, M. P. Nightingale, and M. den Nijs, Quantized hall conductance in a two-dimensional periodic potential, *Phys. Rev. Lett.* **49**, 405 (1982).

[5] D. Xiao, M.-C. Chang, and Q. Niu, Berry phase effects on electronic properties, *Rev. Mod. Phys.* **82**, 1959 (2010).

[6] M. Lohse, C. Schweizer, O. Zilberberg, M. Aidelsburger, and I. Bloch, A thouless quantum pump with ultracold bosonic atoms in an optical superlattice, *Nat. Phys.* **12**, 350 (2016).

[7] S. Nakajima, N. Takei, K. Sakuma, Y. Kuno, P. Marra, and Y. Takahashi, Competition and interplay between topology and quasi-periodic disorder in thouless pumping of ultracold atoms, *Nat. Phys.* **17**, 844 (2021).

[8] Y. E. Kraus, Y. Lahini, Z. Ringel, M. Verbin, and O. Zilberberg, Topological states and adiabatic pumping in quasicrystals, *Phys. Rev. Lett.* **109**, 106402 (2012).

[9] O. Zilberberg, S. Huang, J. Guglielmon, M. Wang, K. P. Chen, Y. E. Kraus, and M. C. Rechtsman, Photonic topological boundary pumping as a probe of 4D quantum Hall physics, *Nature(London)* **553**, 59 (2018).

[10] W. Ma, L. Zhou, Q. Zhang, M. Li, C. Cheng, J. Geng, X. Rong, F. Shi, J. Gong, and J. Du, Experimental observation of a generalized thouless pump with a single spin, *Phys. Rev. Lett.* **120**, 120501 (2018).

[11] M. Jürgensen, S. Mukherjee, and M. C. Rechtsman, Quantized nonlinear Thouless pumping, *Nature (London)* **596**, 63 (2021).

[12] M. Jürgensen and M. C. Rechtsman, Chern number governs soliton motion in nonlinear thouless pumps, *Phys. Rev. Lett.* **128**, 113901 (2022).

[13] Q. Fu, P. Wang, Y. V. Kartashov, V. V. Konotop, and F. Ye, Nonlinear thouless pumping: Solitons and transport breakdown, *Phys. Rev. Lett.* **128**, 154101 (2022).

[14] Q. Fu, P. Wang, Y. V. Kartashov, V. V. Konotop, and F. Ye, Two-dimensional nonlinear thouless pumping of matter waves, *Phys. Rev. Lett.* **129**, 183901 (2022).

[15] N. Mostaan, F. Grusdt, and N. Goldman, Quantized topological pumping of solitons in nonlinear photonics and ultracold atomic mixtures, *Nat. Commun.* **13**, 5997 (2022).

[16] T. Tuloup, R. W. Bomantara, and J. Gong, Breakdown of quantization in nonlinear Thouless pumping, *New J. Phys.* **25**, 083048 (2023).

[17] X. Hu, Z. Li, A.-X. Chen, and X. Luo, Pumping of matter wave solitons in one-dimensional optical superlattices, *New J. Phys.* **26**, 123006 (2024).

[18] H. Lyu, Y. Zhang, and T. Busch, Thouless pumping and trapping of two-component gap solitons, *Phys. Rev. Res.* **6**, L042010 (2024).

[19] A. Szameit and M. C. Rechtsman, Discrete nonlinear topological photonics, *Nat. Phys.* **20**, 905 (2024).

[20] X. Cao, C. Jia, Y. Hu, and Z. Liang, Nonlinear thouless pumping of solitons across an impurity, *Phys. Rev. A* **110**, 013305 (2024).

[21] X. Cao, C. Jia, Y. Hu, and Z. Liang, *Dissipative nonlinear thouless pumping of temporal solitons* (2024), arXiv:2409.03450 [cond-mat.quant-gas].

[22] X. Cao, C. Jia, H. Lyu, Y. Hu, and Z. Liang, Transport of vector solitons in spin-dependent nonlinear thouless pumps, *Phys. Rev. A* **111**, 023329 (2025).

[23] S. Burger, K. Bongs, S. Dettmer, W. Ertmer, K. Sengstock, A. Sanpera, G. V. Shlyapnikov, and M. Lewenstein, Dark solitons in bose-einstein condensates, *Phys. Rev. Lett.* **83**, 5198 (1999).

[24] J. Denschlag, J. E. Simsarian, D. L. Feder, C. W. Clark, L. A. Collins, J. Cubizolles, L. Deng, E. W. Hagley, K. Helmerson, W. P. Reinhardt, S. L. Rolston, B. I. Schneider, and W. D. Phillips, Generating Solitons by Phase Engineering of a Bose-Einstein Condensate, *Science* **287**, 97 (2000).

[25] K. E. Strecker, G. B. Partridge, A. G. Truscott, and R. G. Hulet, Formation and propagation of matter-wave soliton trains, *Nature* **417**, 150 (2002).

[26] B. Wu and Q. Niu, Superfluidity of Bose-Einstein condensate in an optical lattice: Landau-Zener tunnelling and dynamical instability, *New J. Phys.* **5**, 104 (2003).

[27] O. Bleu, D. D. Solnyshkov, and G. Malpuech, Interacting quantum fluid in a polariton chern insulator, *Phys.*

Rev. B **93**, 085438 (2016).

[28] G. Watanabe, B. Venkatesh, and R. Dasgupta, Non-linear Phenomena of Ultracold Atomic Gases in Optical Lattices: Emergence of Novel Features in Extended States, *Entropy* **18**, 118 (2016).

[29] Y. Lumer, Y. Plotnik, M. C. Rechtsman, and M. Segev, Self-localized states in photonic topological insulators, *Phys. Rev. Lett.* **111**, 243905 (2013).

[30] T. Morimoto and N. Nagaosa, Topological nature of nonlinear optical effects in solids, *Sci. Adv.* **2**, e1501524 (2016).

[31] Y. Hadad, A. B. Khanikaev, and A. Alù, Self-induced topological transitions and edge states supported by nonlinear staggered potentials, *Phys. Rev. B* **93**, 155112 (2016).

[32] X. Zhou, Y. Wang, D. Leykam, and Y. D. Chong, Optical isolation with nonlinear topological photonics, *New J. Phys.* **19**, 095002 (2017).

[33] D. Smirnova, D. Leykam, Y. D. Chong, and Y. Kivshar, Nonlinear topological photonics, *Appl. Phys. Rev.* **7**, 021306 (2020).

[34] K. Viebahn, A.-S. Walter, E. Bertok, Z. Zhu, M. Gächter, A. A. Aligia, F. Heidrich-Meisner, and T. Esslinger, Interactions Enable Thouless Pumping in a Nonsliding Lattice, *Phys. Rev. X* **14**, 021049 (2024).

[35] Z. Zhu, Y. Kiefer, S. Jele, M. Gächter, G. Bisson, K. Viebahn, and T. Esslinger, Splitting and Connecting Singlets in Atomic Quantum Circuits, *Phys. Rev. X* **15**, 041032 (2025).

[36] Y. Chen, Q. Fu, Z. Xu, and F. Ye, Progress on New-Type Optical Thouless Pumping, *Laser Photon. Rev.* **n/a**, e01528 (2025).

[37] M. Jürgensen, S. Mukherjee, C. Jörg, and M. C. Rechtsman, Quantized fractional Thouless pumping of solitons, *Nat. Phys.* **19**, 420 (2023).

[38] Y.-L. Tao, Y. Zhang, and Y. Xu, Nonlinearity-induced fractional thouless pumping of solitons, *Phys. Rev. Lett.* **135**, 097202 (2025).

[39] P. St-Jean, V. Goblot, E. Galopin, A. Lemaître, T. Ozawa, L. Le Gratiet, I. Sagnes, J. Bloch, and A. Amo, Lasing in topological edge states of a one-dimensional lattice, *Nat. Photon.* **11**, 651 (2017).

[40] J. M. Zeuner, M. C. Rechtsman, Y. Plotnik, Y. Lumer, S. Nolte, M. S. Rudner, M. Segev, and A. Szameit, Observation of a topological transition in the bulk of a non-hermitian system, *Phys. Rev. Lett.* **115**, 040402 (2015).

[41] Y. Xu, S.-T. Wang, and L.-M. Duan, Weyl exceptional rings in a three-dimensional dissipative cold atomic gas, *Phys. Rev. Lett.* **118**, 045701 (2017).

[42] L. Li, C. H. Lee, and J. Gong, Topological switch for non-hermitian skin effect in cold-atom systems with loss, *Phys. Rev. Lett.* **124**, 250402 (2020).

[43] C. Liang, Y. Tang, A.-N. Xu, and Y.-C. Liu, Observation of exceptional points in thermal atomic ensembles, *Phys. Rev. Lett.* **130**, 263601 (2023).

[44] W. Zhu, X. Fang, D. Li, Y. Sun, Y. Li, Y. Jing, and H. Chen, Simultaneous observation of a topological edge state and exceptional point in an open and non-hermitian acoustic system, *Phys. Rev. Lett.* **121**, 124501 (2018).

[45] Y. Kawakami, A. Kaneta, A. Hashiya, and M. Funato, Impact of radiative and nonradiative recombination processes on the efficiency-droop phenomenon in $in_xga_{1-x}N$ single quantum wells studied by scanning near-field optical microscopy, *Phys. Rev. Appl.* **6**, 044018 (2016).

[46] T. E. Lee, Anomalous edge state in a non-hermitian lattice, *Phys. Rev. Lett.* **116**, 133903 (2016).

[47] S. Yao and Z. Wang, Edge states and topological invariants of non-hermitian systems, *Phys. Rev. Lett.* **121**, 086803 (2018).

[48] F. K. Kunst, E. Edvardsson, J. C. Budich, and E. J. Bergholtz, Biorthogonal bulk-boundary correspondence in non-hermitian systems, *Phys. Rev. Lett.* **121**, 026808 (2018).

[49] T. Yoshida, R. Peters, N. Kawakami, and Y. Hatsugai, Exceptional band touching for strongly correlated systems in equilibrium, *Prog. Theor. Exp. Phys.* **2020**, 12A109 (2020).

[50] K. Yokomizo and S. Murakami, Non-bloch band theory of non-hermitian systems, *Phys. Rev. Lett.* **123**, 066404 (2019).

[51] D. S. Borgnia, A. J. Kruchkov, and R.-J. Slager, Non-hermitian boundary modes and topology, *Phys. Rev. Lett.* **124**, 056802 (2020).

[52] N. Okuma, K. Kawabata, K. Shiozaki, and M. Sato, Topological origin of non-hermitian skin effects, *Phys. Rev. Lett.* **124**, 086801 (2020).

[53] K. Zhang, Z. Yang, and C. Fang, Correspondence between winding numbers and skin modes in non-hermitian systems, *Phys. Rev. Lett.* **125**, 126402 (2020).

[54] B. Zhen, C. W. Hsu, Y. Igarashi, L. Lu, I. Kaminer, A. Pick, S.-L. Chua, J. D. Joannopoulos, and M. Soljačić, Spawning rings of exceptional points out of Dirac cones, *Nature (London)* **525**, 354 (2015).

[55] H. Shen, B. Zhen, and L. Fu, Topological band theory for non-hermitian hamiltonians, *Phys. Rev. Lett.* **120**, 146402 (2018).

[56] T. Yoshida, R. Peters, and N. Kawakami, Non-hermitian perspective of the band structure in heavy-fermion systems, *Phys. Rev. B* **98**, 035141 (2018).

[57] A. A. Zyuzin and A. Y. Zyuzin, Flat band in disorder-driven non-hermitian weyl semimetals, *Phys. Rev. B* **97**, 041203 (2018).

[58] K. Takata and M. Notomi, Photonic topological insulating phase induced solely by gain and loss, *Phys. Rev. Lett.* **121**, 213902 (2018).

[59] J. C. Budich, J. Carlström, F. K. Kunst, and E. J. Bergholtz, Symmetry-protected nodal phases in non-hermitian systems, *Phys. Rev. B* **99**, 041406 (2019).

[60] T. Yoshida, R. Peters, N. Kawakami, and Y. Hatsugai, Symmetry-protected exceptional rings in two-dimensional correlated systems with chiral symmetry, *Phys. Rev. B* **99**, 121101 (2019).

[61] T. Yoshida, T. Mizoguchi, and Y. Hatsugai, Mirror skin effect and its electric circuit simulation, *Phys. Rev. Res.* **2**, 022062 (2020).

[62] T. Yoshida and Y. Hatsugai, Exceptional rings protected by emergent symmetry for mechanical systems, *Phys. Rev. B* **100**, 054109 (2019).

[63] R. Okugawa and T. Yokoyama, Topological exceptional surfaces in non-hermitian systems with parity-time and parity-particle-hole symmetries, *Phys. Rev. B* **99**, 041202 (2019).

[64] H. Zhou, J. Y. Lee, S. Liu, and B. Zhen, Exceptional surfaces in PT-symmetric non-hermitian photonic systems, *Optica* **6**, 190 (2019).

[65] P. Delplace, T. Yoshida, and Y. Hatsugai, Symmetry-protected multifold exceptional points and their topo-

logical characterization, *Phys. Rev. Lett.* **127**, 186602 (2021).

[66] I. Mandal and E. J. Bergholtz, Symmetry and higher-order exceptional points, *Phys. Rev. Lett.* **127**, 186601 (2021).

[67] T. Isobe, T. Yoshida, and Y. Hatsugai, Topological band theory of a generalized eigenvalue problem with hermitian matrices: Symmetry-protected exceptional rings with emergent symmetry, *Phys. Rev. B* **104**, L121105 (2021).

[68] T. Isobe, T. Yoshida, and Y. Hatsugai, A symmetry-protected exceptional ring in a photonic crystal with negative index media, *Nanophotonics* **12**, 2335 (2023).

[69] S. Malzard, C. Poli, and H. Schomerus, Topologically protected defect states in open photonic systems with non-hermitian charge-conjugation and parity-time symmetry, *Phys. Rev. Lett.* **115**, 200402 (2015).

[70] Y. Choi, S. Kang, S. Lim, W. Kim, J.-R. Kim, J.-H. Lee, and K. An, Quasieigenstate coalescence in an atom-cavity quantum composite, *Phys. Rev. Lett.* **104**, 153601 (2010).

[71] T. E. Lee, F. Reiter, and N. Moiseyev, Entanglement and spin squeezing in non-hermitian phase transitions, *Phys. Rev. Lett.* **113**, 250401 (2014).

[72] Y. Ashida, Z. Gong, and M. Ueda, Non-hermitian physics, *Adv. Phys.* **69**, 249 (2020).

[73] B. Gardas, S. Deffner, and A. Saxena, Non-hermitian quantum thermodynamics, *Sci. Rep.* **6**, 23408 (2016).

[74] K. Kawabata, T. Numasawa, and S. Ryu, Entanglement phase transition induced by the non-hermitian skin effect, *Phys. Rev. X* **13**, 021007 (2023).

[75] K. Kawabata, S. Higashikawa, Z. Gong, Y. Ashida, and M. Ueda, Topological unification of time-reversal and particle-hole symmetries in non-Hermitian physics, *Nat. Commun.* **10**, 297 (2019).

[76] J. Li, A. K. Harter, J. Liu, L. De Melo, Y. N. Joglekar, and L. Luo, Observation of parity-time symmetry breaking transitions in a dissipative Floquet system of ultracold atoms, *Nat. Commun.* **10**, 855 (2019).

[77] Z. Ren, D. Liu, E. Zhao, C. He, K. K. Pak, J. Li, and G.-B. Jo, Chiral control of quantum states in non-Hermitian spin-orbit-coupled fermions, *Nat. Phys.* **18**, 385 (2022).

[78] Q. Liang, D. Xie, Z. Dong, H. Li, H. Li, B. Gadway, W. Yi, and B. Yan, Dynamic signatures of non-hermitian skin effect and topology in ultracold atoms, *Phys. Rev. Lett.* **129**, 070401 (2022).

[79] K. Sun and W. Yi, Chiral state transfer under dephasing, *Phys. Rev. A* **108**, 013302 (2023).

[80] W. Chen, M. Abbasi, Y. N. Joglekar, and K. W. Murch, Quantum jumps in the non-hermitian dynamics of a superconducting qubit, *Phys. Rev. Lett.* **127**, 140504 (2021).

[81] W. Chen, M. Abbasi, B. Ha, S. Erdamar, Y. N. Joglekar, and K. W. Murch, Decoherence-induced exceptional points in a dissipative superconducting qubit, *Phys. Rev. Lett.* **128**, 110402 (2022).

[82] L. Xiao, X. Zhan, Z. H. Bian, K. K. Wang, X. Zhang, X. P. Wang, J. Li, K. Mochizuki, D. Kim, N. Kawakami, W. Yi, H. Obuse, B. C. Sanders, and P. Xue, Observation of topological edge states in parity-time-symmetric quantum walks, *Nat. Phys.* **13**, 1117 (2017).

[83] W.-C. Wang, Y.-L. Zhou, H.-L. Zhang, J. Zhang, M.-C. Zhang, Y. Xie, C.-W. Wu, T. Chen, B.-Q. Ou, W. Wu, H. Jing, and P.-X. Chen, Observation of \mathcal{PT} -symmetric quantum coherence in a single-ion system, *Phys. Rev. A* **103**, L020201 (2021).

[84] L. Ding, K. Shi, Q. Zhang, D. Shen, X. Zhang, and W. Zhang, Experimental determination of \mathcal{PT} -symmetric exceptional points in a single trapped ion, *Phys. Rev. Lett.* **126**, 083604 (2021).

[85] Z. Gong, Y. Ashida, K. Kawabata, K. Takasan, S. Higashikawa, and M. Ueda, Topological phases of non-hermitian systems, *Phys. Rev. X* **8**, 031079 (2018).

[86] E. Edvardsson, F. K. Kunst, and E. J. Bergholtz, Non-hermitian extensions of higher-order topological phases and their biorthogonal bulk-boundary correspondence, *Phys. Rev. B* **99**, 081302 (2019).

[87] S. Longhi, Unraveling the non-hermitian skin effect in dissipative systems, *Phys. Rev. B* **102**, 201103 (2020).

[88] L. Pan, X. Chen, Y. Chen, and H. Zhai, Non-Hermitian linear response theory, *Nat. Phys.* **16**, 767 (2020).

[89] J. Li, T. c. v. Prosen, and A. Chan, Spectral statistics of non-hermitian matrices and dissipative quantum chaos, *Phys. Rev. Lett.* **127**, 170602 (2021).

[90] X. Zhan, L. Xiao, Z. Bian, K. Wang, X. Qiu, B. C. Sanders, W. Yi, and P. Xue, Detecting topological invariants in nonunitary discrete-time quantum walks, *Phys. Rev. Lett.* **119**, 130501 (2017).

[91] D. Hao, L. Wang, X. Lu, X. Cao, S. Jia, Y. Hu, and Y. Xiao, Topological atomic spin wave lattices by dissipative couplings, *Phys. Rev. Lett.* **130**, 153602 (2023).

[92] K. Kawabata, K. Shiozaki, M. Ueda, and M. Sato, Symmetry and topology in non-hermitian physics, *Phys. Rev. X* **9**, 041015 (2019).

[93] E. J. Bergholtz, J. C. Budich, and F. K. Kunst, Exceptional topology of non-hermitian systems, *Rev. Mod. Phys.* **93**, 015005 (2021).

[94] C. Poli, M. Bellec, U. Kuhl, F. Mortessagne, and H. Schomerus, Selective enhancement of topologically induced interface states in a dielectric resonator chain, *Nat. Commun.* **6**, 6710 (2015).

[95] M.-A. Miri and A. Alù, Exceptional points in optics and photonics, *Science* **363**, eaar7709 (2019).

[96] S. K. Özdemir, S. Rotter, F. Nori, and L. Yang, Parity-time symmetry and exceptional points in photonics, *Nat. Mater.* **18**, 783 (2019).

[97] Z. Feng and X. Sun, Harnessing dynamical encircling of an exceptional point in anti- \mathcal{PT} -symmetric integrated photonic systems, *Phys. Rev. Lett.* **129**, 273601 (2022).

[98] X. Shu, A. Li, G. Hu, J. Wang, A. Alù, and L. Chen, Fast encirclement of an exceptional point for highly efficient and compact chiral mode converters, *Nat. Commun.* **13**, 2123 (2022).

[99] S. Longhi, Probing non-hermitian skin effect and non-bloch phase transitions, *Phys. Rev. Res.* **1**, 023013 (2019).

[100] A. Kumar, S. Mazumdar, S. D. Mahanti, and K. Saha, Anomalous pumping in the non-Hermitian Rice-Mele model, *J. Phys.: Condens. Matter* **37**, 135601 (2025).

[101] Z. Zhang, T. Li, X.-W. Luo, and W. Yi, Biorthogonal topological charge pumping in non-hermitian systems, *Phys. Rev. B* **109**, 224307 (2024).

[102] M. Ezawa, N. Ishida, Y. Ota, and S. Iwamoto, Nonadiabatic nonlinear non-hermitian quantized pumping, *Phys. Rev. Res.* **6**, 033258 (2024).

[103] K. Kyriakou and K. Moulopoulos, Emergent non-

hermitian boundary contributions to charge pumping and electric polarization (2021), arXiv:2106.14173 [cond-mat.mes-hall].

[104] Z. Fedorova, H. Qiu, S. Linden, and J. Kroha, Observation of topological transport quantization by dissipation in fast Thouless pumps, *Nat. Commun.* **11**, 3758 (2020).

[105] C. Yuce, Spontaneous topological pumping in non-hermitian systems, *Phys. Rev. A* **99**, 032109 (2019).

[106] B. Höckendorf, A. Alvermann, and H. Fehske, Topological origin of quantized transport in non-hermitian floquet chains, *Phys. Rev. Res.* **2**, 023235 (2020).

[107] X. Yang, C. Tan, Y. Yan, and R. Zhang, Non-hermitian thouless pumping: Interplay between topological charge pumping and directional tunneling, *Phys. Rev. A* **111**, 053308 (2025).

[108] G.-F. Guo, X.-X. Bao, and L. Tan, Non-Hermitian bulk-boundary correspondence and singular behaviors of generalized Brillouin zone, *New J. Phys.* **23**, 123007 (2021).

[109] X. Ji and X. Yang, Generalized bulk-boundary correspondence in periodically driven non-Hermitian systems, *J. Phys.: Condens. Matter* **36**, 243001 (2024).

[110] Z. Yang, K. Zhang, C. Fang, and J. Hu, Non-hermitian bulk-boundary correspondence and auxiliary generalized brillouin zone theory, *Phys. Rev. Lett.* **125**, 226402 (2020).

[111] S. Xia, D. Kaltsas, D. Song, I. Komis, J. Xu, A. Szameit, H. Buljan, K. G. Makris, and Z. Chen, Nonlinear tuning of PT symmetry and non-hermitian topological states, *Science* **372**, 72 (2021).

[112] V. V. Konotop, J. Yang, and D. A. Zezyulin, Nonlinear waves in \mathcal{PT} -symmetric systems, *Rev. Mod. Phys.* **88**, 035002 (2016).

[113] T. Isobe, T. Yoshida, and Y. Hatsugai, Bulk-edge correspondence for nonlinear eigenvalue problems, *Phys. Rev. Lett.* **132**, 126601 (2024).

[114] C. Bai and Z. Liang, Anomalous bulk-edge correspondence of the nonlinear rice-mele model, *Phys. Rev. A* **111**, 042201 (2025).

[115] C. Bai and Z. Liang, Fractional thouless pumping of solitons: A unique manifestation of bulk-edge correspondence of nonlinear eigenvalue problems, *Phys. Rev. A* **112**, 052207 (2025).

[116] M. J. Rice and E. J. Mele, Elementary excitations of a linearly conjugated diatomic polymer, *Phys. Rev. Lett.* **49**, 1455 (1982).

[117] S. Wang, B. Wang, C. Liu, C. Qin, L. Zhao, W. Liu, S. Longhi, and P. Lu, Nonlinear non-hermitian skin effect and skin solitons in temporal photonic feedforward lattices, *Phys. Rev. Lett.* **134**, 243805 (2025).

[118] K. Kawabata and D. Nakamura, Hopf bifurcation of nonlinear non-hermitian skin effect, *Phys. Rev. Lett.* **135**, 126610 (2025).

[119] S. Cheng, Y. Jiang, and G. Xianlong, Bulk-edge correspondence for the nonlinear eigenvalues problem of the haldane model, *Phys. Rev. B* **109**, 134201 (2024).

[120] A. Alexandradinata, X. Dai, and B. A. Bernevig, Wilson-loop characterization of inversion-symmetric topological insulators, *Phys. Rev. B* **89**, 155114 (2014).